



## 1 Site specific parameterizations of longwave radiation

2 Giuseppe Formetta<sup>1</sup>, Marialaura Bancheri<sup>2</sup>, Olaf David<sup>3</sup> and Riccardo Rigon<sup>2</sup>

3 <sup>1</sup>Centre for Ecology & Hydrology, Crowmarsh Gifford, Wallingford, UK

4 <sup>2</sup>Dipartimento di Ingegneria Civile Ambientale e Meccanica, Universita' degli Studi di Trento,  
5 Italy

6 <sup>3</sup>Dept. of Civil and Environmental Engineering, Colorado State University, Fort Collins, CO,  
7 USA

8 May 30, 2016

### 9 Abstract

10 In this work ten algorithms for estimating downwelling longwave atmospheric radiation ( $L_{\downarrow}$ ) and one  
11 for upwelling longwave radiation ( $L_{\uparrow}$ ) are integrated into the hydrological model JGrass-NewAge. The  
12 algorithms are tested against energy flux measurements available for twenty-four sites in North America to  
13 assess their reliability. These new JGrass-NewAge model components are used i) to evaluate the performances  
14 of simplified models (SMs) of  $L_{\downarrow}$ , as presented in literature formulations, and ii) to determine by automatic  
15 calibration the site-specific parameter sets for SMs of  $L_{\downarrow}$ . For locations where calibration is not possible  
16 because of a lack of measured data, we perform a multiple regression using on-site variables, such as mean  
17 annual air temperature, relative humidity, precipitation, and altitude. The regressions are verified through  
18 a leave-one-out cross validation, which also gathers information about the possible errors of estimation.  
19 Most of the SMs, when executed with parameters derived from the multiple regressions, give enhanced  
20 performances compared to the corresponding literature formulation. A sensitivity analysis is carried out for  
21 each SM to understand how small variations of a given parameter influence SM performance. Regarding  
22 the  $L_{\downarrow}$  simulations, the Brunt (1932) and Idso (1981) SMs, in their literature formulations, provide the  
23 best performances in many of the sites. The site-specific parameter calibration improves SM performances  
24 compared to their literature formulations. Specifically, the root mean square error (RMSE) is almost halved  
25 and the Kling Gupta efficiency is improved at all sites.

26 The  $L_{\uparrow}$  SM is tested by using three different temperatures (surface soil temperature, air temperature at  
27 2 m elevation, and soil temperature at 4 cm depth) and model performances are then assessed. Results show  
28 that the best performances are achieved using the surface soil temperature and the air temperature.

29 Models and regression parameters are available for any use, as specified in the paper.



## 30 1 Introduction

31 Longwave radiation (1-100  $\mu\text{m}$ ) is an important component of the radiation balance on earth and it affects many  
32 phenomena, such as evapotranspiration, snow melt (Plüss and Ohmura, 1997), glacier evolution (MacDonell  
33 et al., 2013), vegetation dynamics (Rotenberg et al., 1998), plant respiration, and primary productivity (Leigh Jr,  
34 1999). Longwave radiation is usually measured with very expensive pyrgeometers, but these are not normally  
35 available in basic meteorological stations, even though an increasing number of projects has been developed to  
36 fill the gap, Augustine et al. (2000), as seen in Augustine et al. (2005) and Baldocchi et al. (2001). The use of  
37 satellite products to estimate longwave solar radiation is increasing (GEWEX, Global Energy and Water cycle  
38 Experiment, ISCCP the International Satellite Cloud Climatology Project) but they have too coarse a spatial  
39 resolution for many hydrological uses. Therefore, models have been developed to solve energy transfer equations  
40 and compute radiation at the surface, e.g. Key and Schweiger (1998), Kneizys et al. (1988). These physically  
41 based and fully distributed models provide accurate estimates of the radiation components. However, they  
42 require input data and model parameters that are not easily available. To overcome this issue, simplified models  
43 (SM), which are based on empirical or physical conceptualizations, have been developed to relate longwave  
44 radiation to atmospheric proxy data such as air temperature, deficit of vapor pressure, and shortwave radiation.  
45 They are widely used and provide clear sky (e.g. Ångström (1915); Brunt (1932); Idso and Jackson (1969)) and  
46 all-sky estimations of downwelling,  $L_{\downarrow}$ , and upwelling,  $L_{\uparrow}$ , longwave radiation (e.g. Brutsaert (1975); Iziomon  
47 et al. (2003a)).

48 SM performances have been assessed in many studies by comparing measured and modeled  $L_{\downarrow}$  at hourly  
49 and daily time-steps (e.g. Sugita and Brutsaert (1993b); Iziomon et al. (2003b); Juszak and Pellicciotti (2013)).  
50 Hatfield et al. (1983) was among the first to present a comparison of the most used SMs in an evaluation of  
51 their accuracy. It tested seven clear-sky algorithms using atmospheric data from different stations in the United  
52 States. So In order to validate the SMs under different climatic conditions, they performed linear regression  
53 analyses on the relationship between simulated and measured  $L_{\downarrow}$  for each algorithm. The results of the study  
54 show that the best models were Brunt (1932), Brutsaert (1975) and Idso (1981). Flerchinger et al. (2009)  
55 made a similar comparison using more formulations (13) and a wider data-set from North America and China,  
56 considering all possible sky conditions. Finally, Carmona et al. (2014) evaluated the performance of six SMs,  
57 with both literature and site-specific formulations, under clear-sky conditions for the sub-humid Pampean region  
58 of Argentina. However, none of the above studies have provided a comprehensive set of open-source tools that  
59 are well documented and ready for practical use by other researchers and practitioners.

60 This paper introduces the LongWave Radiation Balance package (LWRB) of the JGrass-NewAge modelling  
61 system Formetta et al. (2014a). LWRB implements 10 formulations for  $L_{\downarrow}$  and one for  $L_{\uparrow}$  longwave radiation.  
62 The package was systematically tested against measured  $L_{\downarrow}$  and  $L_{\uparrow}$  longwave radiation data from 24 stations  
63 across the USA, chosen from the 65 stations of the AmeriFlux Network. Unlike all previous works, the LWRB  
64 component follows the specifications of the Object Modeling System (OMS) framework, David et al. (2013).  
65 Therefore, it can use all of the JGrass-NewAge tools for the automatic calibration algorithms, data management



66 and GIS visualization, and it can be seamlessly integrated into various modeling solutions for the estimation of  
67 water budget fluxes (Formetta et al., 2014a).

68 The paper is organized into five sections, with Section 1 being this introduction. Section 2 describes method-  
69 ology, calibration and verification for the  $L_{\downarrow}$  and  $L_{\uparrow}$  models. Section 3 presents the study sites and the datasets  
70 used. Section 4 presents the simulation results for  $L_{\downarrow}$  and  $L_{\uparrow}$  longwave radiation. It includes model verification  
71 and calibration, sensitivity analysis and multiple regressions of the parameters against some explaining variables  
72 for  $L_{\downarrow}$ . It also presents a verification of the  $L_{\uparrow}$  model, which includes an assessment of the model performances  
73 in predicting correct upwelling longwave  $L_{\uparrow}$  radiation in using different temperatures (soil surface temperature,  
74 air temperature, and soil temperature at 4 cm below surface). In Section 5 we present our conclusions.

## 75 2 Methodology

76 The SMs for  $L_{\uparrow}$  [ $\text{Wm}^{-2}$ ] and  $L_{\downarrow}$  [ $\text{Wm}^{-2}$ ] longwave radiation are based on the Stefan-Boltzmann equation:

$$L_{\downarrow} = \epsilon_{all-sky} \cdot \sigma \cdot T_a^4 \quad (1)$$

$$L_{\uparrow} = \epsilon_s \cdot \sigma \cdot T_s^4 \quad (2)$$

77 where  $\sigma = 5.670 \cdot 10^{-8}$  [ $\text{Kg s}^{-3} \text{K}^{-4}$ ] is the Stefan-Boltzmann constant,  $T_a$  [K] is the near-surface air  
78 temperature,  $\epsilon_{all-sky}$  [-] is the effective atmospheric emissivity,  $\epsilon_s$  [-] is the soil emissivity and  $T_s$  [K] is the  
79 surface soil temperature. To account for the increase of  $L_{\downarrow}$  in cloudy conditions,  $\epsilon_{all-sky}$  [-] is formulated  
80 according to eq. (3):

$$\epsilon_{all-sky} = \epsilon_{clear} \cdot (1 + a \cdot c^b) \quad (3)$$

81 where  $c$  [-] is the clearness index and  $a$  [-] and  $b$  [-] are two calibration coefficients. Site specific values of  $a$   
82 and  $b$  are presented in Brutsaert (1975), ( $a=0.22$  and  $b=1$ ), Iziomon et al. (2003a) ( $a$  ranges between 0.25 and  
83 0.4 and  $b=2$ ) and Keding (1989) ( $a=0.183$  and  $b=2.18$ ). In our modeling system  $a$  and  $b$  are calibrated to fit  
84 measurement data under all-sky conditions. The cloud cover fraction,  $c$ , can be estimated from solar radiation  
85 measurements (Crawford and Duchon, 1999), from visual observations (Alados-Arboledas et al., 1995, Niemelä  
86 et al., 2001), and from satellite data (Sugita and Brutsaert, 1993a) or it can be modeled as well. In this study  
87 we use the formulation presented in Campbell (1985) and Flerchinger (2000), where  $c$  is related to the clearness  
88 index, (i.e. the ratio between the measured incoming solar radiation,  $I_m$  [ $\text{Wm}^{-2}$ ], and the theoretical solar  
89 radiation computed at the top of the atmosphere,  $I_{top}$  [ $\text{Wm}^{-2}$ ]). This type of formulation needs a shortwave  
90 radiation balance model to estimate  $I_{top}$  and meteorological stations to measure  $I_m$ ; also, it cannot estimate  $c$   
91 at night. In our application, the fact that the SMs are fully integrated into the JGrass-NewAge system allows  
92 us to use the shortwave radiation balance model (Formetta et al., 2013) to compute  $I_{top}$ . Night-time values of  
93  $c$  are computed with a linear interpolation between its values at the last hour of daylight and the first hour of



daylight on consecutive days. Ten SMs from literature have been implemented for the computation of  $\epsilon_{clear}$ .  
 Table 1 specifies assigned component number, component name, defining equation, and reference to the paper  
 from which it is derived. X, Y and Z are the parameters provided in literature for each model, listed in table 2.

ID	Name	Formulation	Reference
1	Angstrom	$\epsilon_{clear} = X - Y \cdot 10^{Ze}$	Angstrom [1918]
2	Brunt's	$\epsilon_{clear} = X + Y \cdot e^{0.5}$	Brunt's [1932]
3	Swinbank	$\epsilon_{clear} = X \cdot 10^{-13} \cdot T_a^6$	Swinbank [1963]
4	Idso and Jackson	$\epsilon_{clear} = 1 - X \cdot \exp(-Y \cdot 10^{-4} \cdot (273 - T_a)^2)$	Idso and Jackson [1969]
5	Brutsaert	$\epsilon_{clear} = X \cdot (e/T_a)^{1/Z}$	Brutsaert [1975]
6	Idso	$\epsilon_{clear} = X + Y \cdot 10^{-4} \cdot e \cdot \exp(1500/T_a)$	Idso [1981]
7	Monteith and Unsworth	$\epsilon_{clear} = X + Y \cdot \sigma \cdot T_a^4$	Monteith and Unsworth [1990]
8	Konzelmann	$\epsilon_{clear} = X + Y \cdot (e/T_a)^{1/8}$	Konzelmann et al [1994]
9	Prata	$\epsilon_{clear} = [1 - (X + w) \cdot \exp(-(Y + Z \cdot w)^{1/2})]$	Prata [1996]
10	Dilley and O'Brien	$\epsilon_{clear} = X + Y \cdot (T_a/273.16)^6 + Z \cdot (w/25)^{1/2}$	Dilley and O'Brien [1998]

**Table 1:** Clear sky emissivity formulations:  $T_a$  is the air temperature [K],  $w$  [ $kg/m^2$ ] is precipitable water =  $4650 [e_0/T_a]$  and  $e$  [kPa] is screen-level water-vapour pressure.

The models presented in table 1 were proposed with coefficient values (X, Y, Z) strictly related to the location  
 in which the authors applied the model and where measurements of  $L_{\downarrow}$  radiation were collected. Coefficients  
 reflect climatic, atmospheric and hydrological conditions of the sites, and are reported in Table 2.

ID	Name	X	Y	Z
1	Angstrom	0.83	0.18	-0.07
2	Brunt	0.52	0.21	[-]
3	Swinbank	5.31	[-]	[-]
4	Idso and Jackson	0.26	-7.77	[-]
5	Brutsaert	1.72	7	[-]
6	Idso	0.70	5.95	[-]
7	Monteith and Unsworth	-119.00	1.06	[-]
8	Konzelmann et al	0.23	0.48	[-]
9	Prata	1.00	1.20	3.00
10	Dilley and O'brien	59.38	113.70	96.96

**Table 2:** Model parameter values as presented in their literature formulation.

The formulation of the  $L_{\uparrow}$  requires the soil emissivity, which usually is a property of the nature of a surface,  
 and the surface soil temperature. Table 3 shows the literature values(Brutsaert, 2005) of the soil emissivity for  
 different surface types:  $\epsilon_s$  varies from a minimum of 0.95 for bare soils to a maximum of 0.99 for fresh snow.

Nature of surface	Emissivity
Bare soil (mineral)	0.95 – 0.97
Bare soil (organic)	0.97 – 0.98
Grassy vegetation	0.97 – 0.98
Tree vegetation	0.96 – 0.97
Snow (old)	0.97
Snow (fresh)	0.99

**Table 3:** Soil emissivity for surface types (Brutsaert, 2005).

Since surface soil temperature measurements are only available at a few measurement sites, if the difference  
 between soil and air temperatures is not too big, it is possible to simulate  $L_{\uparrow}$  using the air temperature, Park  
 et al. (2008). In our approach three different types of temperature were used to simulate  $L_{\uparrow}$ , specifically: surface



106 soil temperature; air temperature at 2 m height; and soil temperature at 4 cm depth.

107 The LWRB package (see flowchart in figure1) is part of the JGrass-NewAge system and was preliminary  
 108 tested in Formetta et al. (2014b). Model inputs depend on the specific SM being implemented and the purpose  
 109 of the run being performed (calibration, verification, simulation). The inputs are meteorological observations  
 110 such as air temperature, relative humidity, incoming solar radiation, and sky clearness index. The LWRB is also  
 111 fed by other JGrass-NewAGE components, such as the shortwave radiation balance (SWRB) (Formetta et al.,  
 112 2013). To test model performances (i.e. verification), the LWRB can be connected to the system's Verification  
 113 component; to execute the parameter calibration algorithm (Formetta et al., 2014a), it can be connected to the  
 114 LUCA (Let Us CALibrate) component. In turn, all these components can and/or need to be connected to other  
 115 ones, as the problem under examination may require.

116 Further information about the SMs used is available in table 1 and in Carmona et al. (2014).

117 Model outputs are  $L_{\downarrow}$  and  $L_{\uparrow}$ . These can be provided in single points of specified coordinates or over a  
 118 whole geographic area, represented as a raster map. For the latter case a digital elevation model (DEM) of the  
 119 study area is necessary in input.

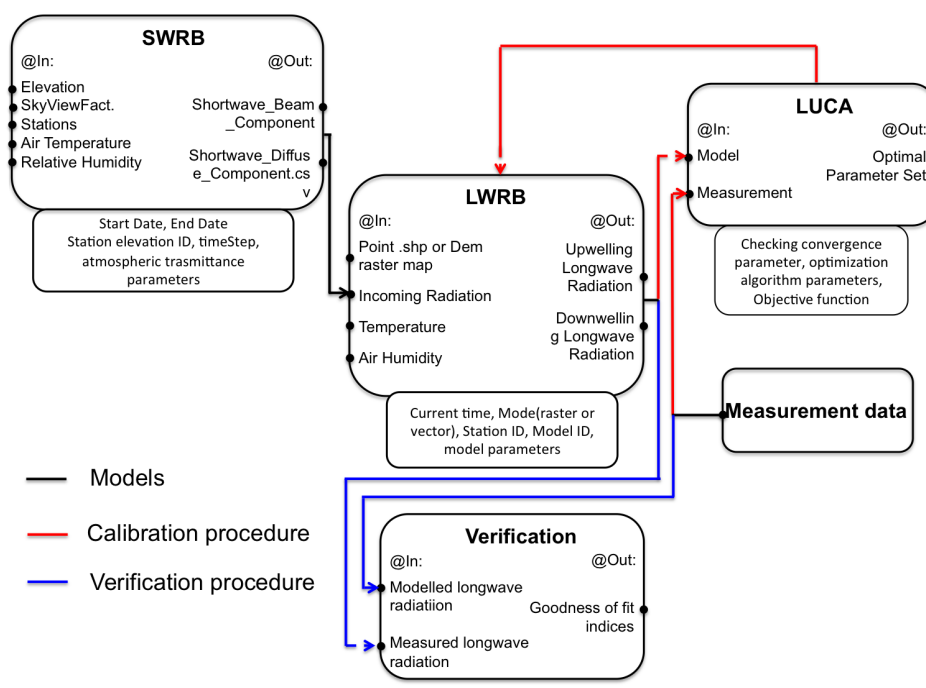


Figure 1: The LWRB component of JGrass-NewAge and the flowchart to model longwave radiation.

## 120 2.1 Calibration of $L_{\downarrow}$ longwave radiation models

121 Model calibration estimates the site-specific parameters of  $L_{\downarrow}$  models by tweaking them with a specific algorithm  
 122 in order to best fit measured data. To this end, we use the LUCA calibration algorithm proposed in (Hay et al.,



2006), which is a part of the OMS core and is able to optimize parameters of any OMS component. LUCA is a multiple-objective, stepwise, and automated procedure. As with any automatic calibration algorithm, it is based on two elements: a global search algorithm; and the objective function(s) to evaluate model performance. In this case, the global search algorithm is the Shuffled Complex Evolution, which has been widely used and described in literature (e.g., Duan et al., 1993). As the objective function we use the Kling-Gupta Efficiency (KGE), which is described below, but LUCA could use other objective functions just as well.

The calibration procedure for  $L_{\downarrow}$  follows these steps:

- The theoretical solar radiation at the top of the atmosphere ( $I_{top}$ ) is computed using the SWRB (see Figure 1);
- The clearness index,  $c$ , is calculated as the ratio between the measured incoming solar radiation ( $I_m$ ) and  $I_{top}$ ;
- Clear-sky and cloud-cover hours are detected by a threshold on the clearness index (equal to 0.6), providing two subsets of measured  $L_{\downarrow}$ , which are  $L_{\downarrow clear}$  and  $L_{\downarrow cloud}$ ;
- The parameters X, Y, and Z for the models in table 1 are optimised using the subset  $L_{\downarrow clear}$  and setting  $a=0$  in eq. 3.
- The parameters  $a$  and  $b$  for eq. 3 are optimized using the subset  $L_{\downarrow cloud}$  and using the X, Y, and Z values computed in the previous step.

The calibration procedure provides the optimal set of parameters at a given location for each of the ten models.

As well as parameter calibration, we carry out a model parameter sensitivity analysis and we provide a linear regression model relating a set of site-specific optimal parameters with easily available climatic variables, such as mean air temperature, relative humidity, precipitation and altitude.

## 2.2 Verification of $L_{\downarrow}$ and $L_{\uparrow}$ longwave radiation models

As presented in previous applications (e.g. Hatfield et al. (1983), Flerchinger et al. (2009)), we use the SMs with the original coefficients from literature (i.e. the parameters of table 2) and compare the performances of the models against available measurements of  $L_{\downarrow}$  and  $L_{\uparrow}$  for each site. The goodness of fit is evaluated by using two goodness-of-fit estimators: the Kling-Gupta Efficiency (KGE) presented in Gupta et al. (2009); and the root mean square error (RMSE).

The KGE (eq. 4) is able to incorporate into one objective function three different statistical measures of the relation between measured (M) and simulated (S) data: (i) the correlation coefficient,  $r$ ; (ii) the variability error,  $a = \sigma_S/\sigma_M$ ; and (iii) the bias error,  $b = \mu_S/\mu_M$ . In these definitions  $\mu_S$  and  $\mu_M$  are the mean values, while  $\sigma_S$  and  $\sigma_M$  are the standard deviations, of measured and simulated time series.

$$KGE = 1 - \sqrt{(r-1)^2 + (a-1)^2 + (b-1)^2} \quad (4)$$



155 The RMSE, on the other hand, is presented in eq. 5:

$$RMSE = \sqrt{\frac{1}{N} \sum_{i=1}^N (M_i - S_i)^2} \quad (5)$$

156 where M and S represents the measured and simulated data respectively.

### 157 3 The study area: the AmeriFlux Network

158 To test and calibrate the LWRB SMs we use twenty-four meteorological stations of the AmeriFlux Network  
159 (<http://ameriflux.ornl.gov>). AmeriFlux is a network of sites that measure water, energy, and CO<sub>2</sub> ecosystem  
160 fluxes in North and South America. The dataset is widely known and used for biological and environmental  
161 applications. To cite a few, Xiao et al. (2010) used Ameriflux data in a study on gross primary production data,  
162 Kelliher et al. (2004) in a study on carbon mineralization, and Barr et al. (2012) in a study on hurricanes. Data  
163 used in this study are the Level 2, 30-minute average data. Complete descriptions and downloads are available  
164 at the Web interface located at <http://public.ornl.gov/ameriflux/>.

165 We have chosen twenty-four sites that are representative of most of the USA and span a wide climatic range:  
166 going from the arid climate of Arizona, where the average air temperature is 16 °C and the annual precipitation  
167 is 350 mm, to the equatorial climate of Florida, where the average air temperature is 24 °C and the annual  
168 precipitation is 950 mm. Some general and climatic characteristics for each site are summarized in table 4, while  
169 figure 2 shows their locations. The 30-minute average data have been cumulated to obtain continuous time series  
170 of averaged, hourly data for longwave radiation, air and soil temperature, relative humidity, precipitation, and  
171 soil water content.

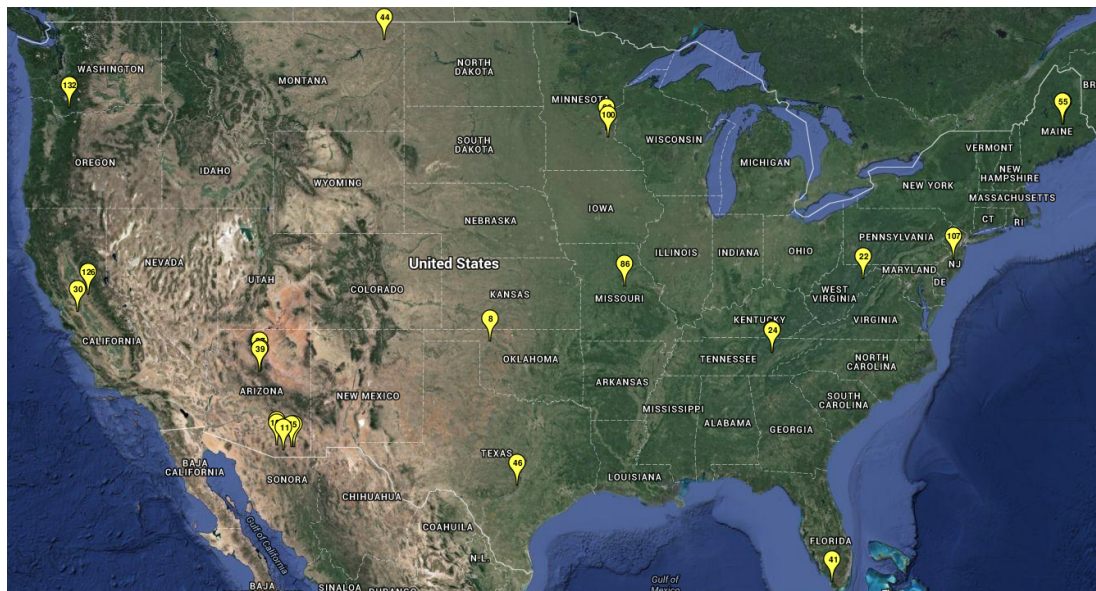


Figure 2: Test site locations in the United State of America.



SiteID	State	Latitude	Longitude	Elevation (m)	Climate	T (°C)	Data period
1	AZ	31.908	-110.840	991	semiarid	19	2008 – 2013
2	AZ	31.591	-110.509	1469	temperate,arid	16	2002 – 2011
3	AZ	31.744	-110.052	1372	temperate,semi-arid	17	2007 – 2013
4	AZ	31.737	-109.942	1531	temperate,semi-arid	17	2004 – 2013
5	AZ	31.821	-110.866	116	subtropical	19	2004 – 2014
6	AZ	35.445	-111.772	2270	warm temperate	9	2005 – 2010
7	AZ	35.143	-111.727	2160	warm temperate	9	2005 – 2010
8	AZ	35.089	-111.762	2180	warm temperate	8	2005 – 2010
9	CA	37.677	-121.530	323	mild	16	2010 – 2012
10	CA	38.407	-120.951	129	mediterranean	15	2000 – 2012
11	FL	25.365	-81.078	0	equatorial savannah	24	2004 – 2011
12	ME	45.207	-68.725	61	temperate continental	5	1996 – 2008
13	ME	45.204	-68.740	60	temperate continental	6	1996 – 2009
14	MN	44.995	-93.186	301	continental	6	2005 – 2009
15	MN	44.714	-93.090	260	snowy, humid summer	8	2003 – 2012
16	MO	38.744	-92.200	219	temperate continental	13	2004 – 2013
17	MT	48.308	-105.102	634	continental	5	2000 – 2008
18	NJ	39.914	-74.596	30	temperate	12	2005 – 2012
19	OK	36.427	-99.420	611	cool temperate	15	2009 – 2012
20	TN	35.931	-84.332	286	temperate continental	15	2005 – 2011
21	TN	35.959	-84.287	343	temperate	14	1994 – 2007
22	TX	29.940	-97.990	232	warm temperate	20	2004 – 2012
23	WA	45.821	-121.952	371	strongly seasonal	9	1998 – 2013
24	WV	39.063	-79.421	994	temperate	7	2004 – 2010

**Table 4:** Some general and climatic characteristics of the sites used for calibration: elevation is the site elevation above sea level, T is the annual average temperature, and data period refers to the period of available measurements.

## 172 4 Results

### 173 4.1 Verification of $L_{\perp}$ models with literature parameters

174 When implementing the ten  $L_{\perp}$  SMs using the literature parameters, in many cases, they show a strong bias in  
 175 reproducing measured data. A selection of representative cases is presented in Figure 3, which shows scatterplots  
 176 for four SMs in relation to one measurement station. The black points represent the hourly estimates of  $L_{\perp}$   
 177 provided by literature formulations, while the solid red line represents the line of optimal predictions. Model 1  
 178 (Ångström (1915)) shows a tendency to lie below the 45 degree line, indicating a negative bias (percent bias of  
 179 -9.8) and, therefore, an underestimation of  $L_{\perp}$ . In contrast, model 9 (Prata (1996)) shows an overestimation of  
 180  $L_{\perp}$  with a percent bias value of 26.3.

181 Figure 4 presents the KGE (first column) and RMSE (second column) obtained for each model under clear-  
 182 sky conditions, grouped by classes of latitude and longitude. Model 8 (Konzelmann et al. (1994)) does not  
 183 perform very well for some reason. Its KGE values range between 0.16 and 0.41, while its RMSE values are  
 184 higher than  $100 W/m^2$ , with a maximum of  $200 W/m^2$ . Model 6 (Idso (1981)) and model 2 (Brunt (1932))  
 185 provide the best results, independently of the latitude and longitude ranges where they are applied. Their KGE  
 186 values are between 0.75 and 0.94, while the RMSE has a maximum value of  $39 W/m^2$ .

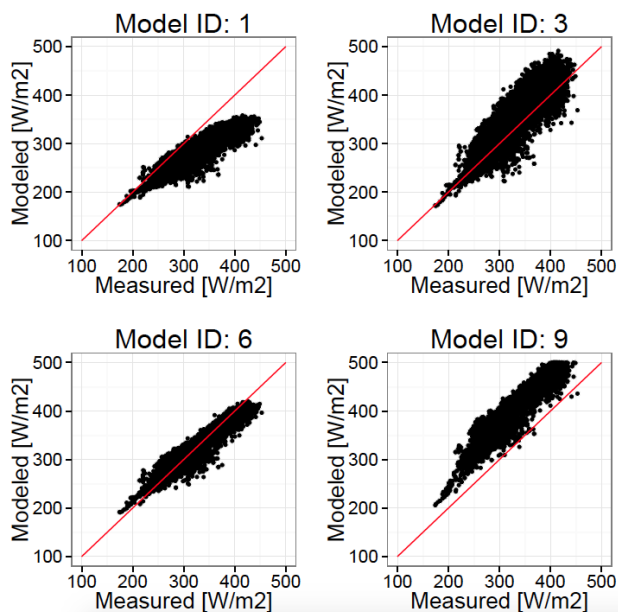


**Figure 3:** Results of the clear-sky simulation for four literature models using data from Howland Forest (Maine).

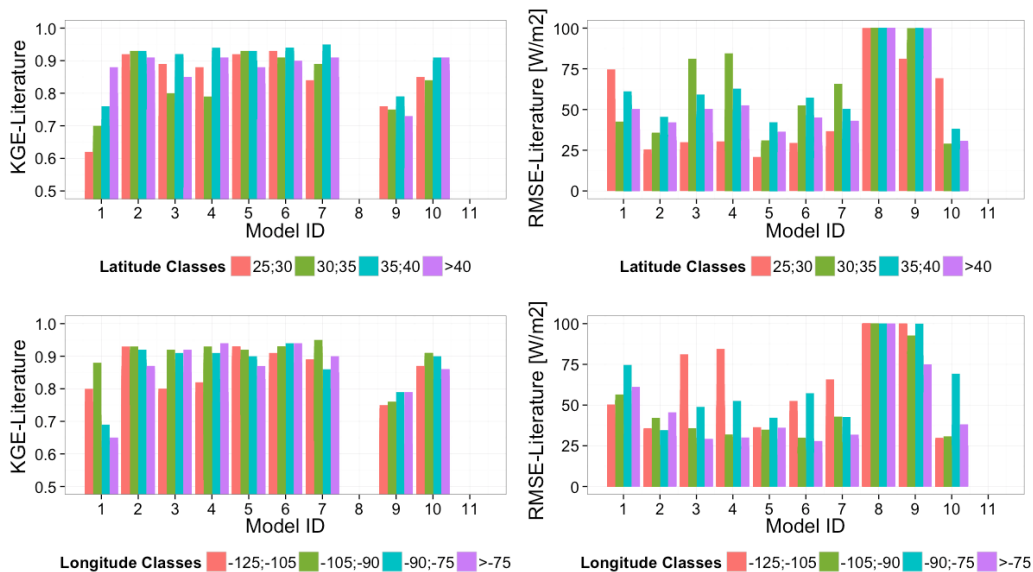


**Figure 4:** KGE and RMSE values for each clear-sky simulation using literature formulations, grouped by classes of latitude and longitude. The values of the KGE shown are those above 0.5: in this case, model 8 KGE values are not represented as they are between 0.16 and 0.41. The range of RMSE is 0-100  $W/m^2$ .



## 187 4.2 $L_1$ models with site-specific parameters

188 The calibration procedure greatly improves the performances of all ten SMs. Optimized model parameters for  
 189 each model are reported in the supplementary material. Figure 5 presents the KGE and RMSE values for  
 190 clear-sky conditions grouped by classes of latitude and longitude. The percentage of KGE improvement ranges  
 191 from its maximum value of 80% for model 8 (which is not, however, representative of the mean behavior of  
 192 the SMs) to less than 10% for model 6, with an average improvement of around 35%. Even though variations  
 193 in model performances with longitude and latitude classes still exist when using optimized model parameters,  
 194 the magnitude of these variations is reduced with respect to the use of literature formulations. The calibration  
 195 procedure reduces the RMSE values for all the models to below  $50 \text{ W/m}^2$ , with the exception of model 8, which  
 196 now has a maximum of  $58 \text{ W/m}^2$ .

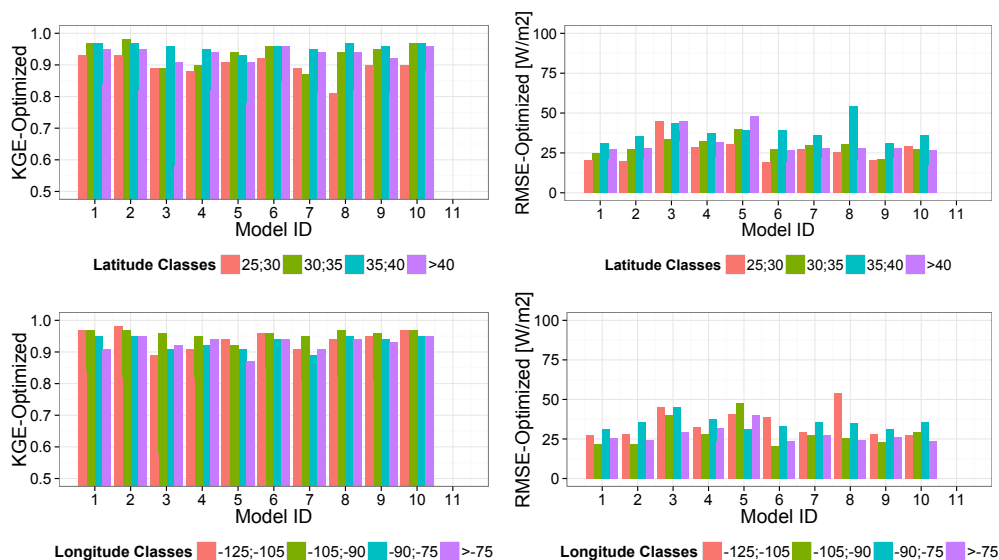


**Figure 5:** KGE (best is 1) and RMSE (best is 0) values for each optimized formulation in clear-sky conditions, grouped by classes of latitude and longitude. Only values of KGE above 0.5 are shown.

197 Figure 6 presents KGE and RMSE values for each model under all-sky conditions, grouped by latitude and  
 198 longitude classes. In general, for all-sky conditions we observe a deterioration of KGE and RMSE values with  
 199 respect to the clear-sky optimized case, with a decrease in KGE values up to a maximum of 25% for model 10.  
 200 This may be due to uncertainty incorporated in the formulation of the cloudy-sky correction model (eq. 3): it  
 201 seems that sometimes the cloud effects are not accounted for appropriately. This, however, is in line with the  
 202 findings of Carmona et al. (2014).

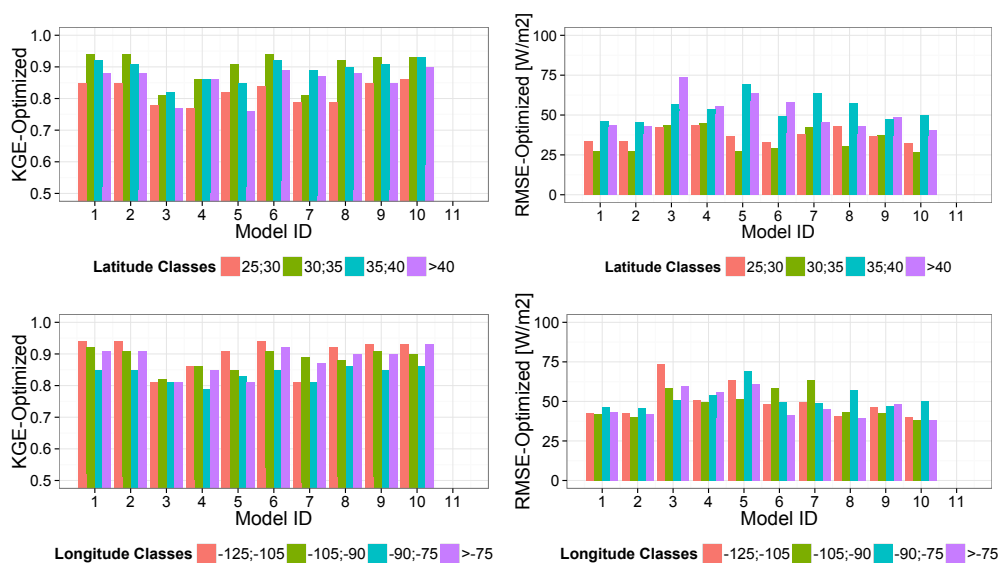


**Figure 6:** KGE and RMSE values for each model in all-sky conditions, grouped by classes of latitude and longitude. Only values of KGE above 0.5 are shown.

### 203 4.3 Sensitivity analysis of $L_{\perp}$ models

204 For each  $L_{\perp}$  model we carry out a model parameters sensitivity analysis to investigate the effects and significance  
 205 of parameters on performance for different model structures (i.e. models with one, two, and three parameters).  
 206 The analyses are structured according to the following steps:

- 207 • we start with the optimal parameter set, computed by the optimization process for the selected model;
- 208 • all parameters are kept constant and equal to the optimal parameter set, except for the parameter under  
 209 analysis;
- 210 • 1000 random values of the analyzed parameter are picked from a uniform distribution centered on the  
 211 optimal value with width equal to  $\pm 30\%$  of the optimal value; in this way 1000 model parameter sets  
 212 were defined and 1000 model runs were performed;
- 213 • 1000 values of KGE are computed by comparing the model outputs with measured time series.

214 The procedure was repeated for each parameter of each model. Figures 7-a and 7-b summarize the sensitivity  
 215 analysis results for models 1 to 5 and models 6 to 10, respectively. Each figure presents three columns, one for  
 216 each parameter. Considering model 1 and parameter X: the range of X is subdivided into ten equal-sized classes  
 217 and for each class the corresponding KGE values are presented as a boxplot. A smooth blue line passing through  
 218 the boxplot medians is added to highlight any possible pattern to parameter sensitivity. A flat line indicates that  
 219 the model is not sensitive to parameter variation about optimal value. Results suggest that models with one  
 220 and two parameters are all sensitive to parameter variation, presenting a peak in KGE in correspondence with  
 221 their optimal values; this is more evident in models with two parameters. Models with three parameters tend

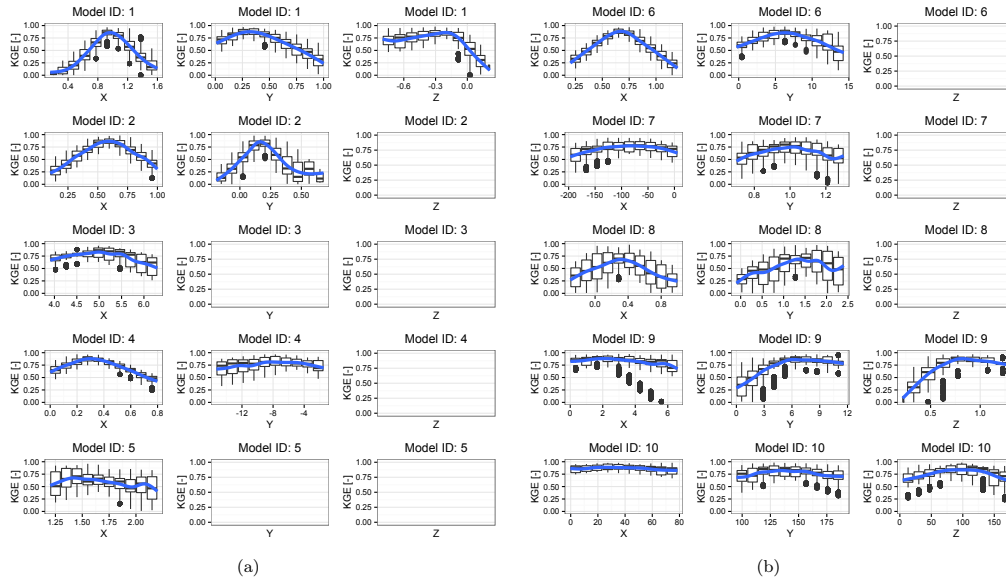


Figure 7: Results of the model parameters sensitivity analysis.

to have at least one insensitive parameter, except for model 1, that could reveal a possible overparameterization of the modeling process.

#### 4.4 Regression model for parameters of $L_4$ models

The calibration procedure that allows the estimation of site specific parameters for  $L_4$  models requires measured downwelling longwave data. Because these measurements are rarely available, we implement a straightforward multivariate linear regression (Chambers et al., 1992; Wilkinson and Rogers, 1973) to relate the site-specific parameters X, Y and Z to a set of easily available site specific climatic variables, used as regressors  $r_i$ . To perform the regression we use the open-source R software (<https://cran.r-project.org>) and to select the best regressors we use algorithms known as "best subsets regression", which are available in all common statistical software packages. The script containing the regression model is available, with the complementary material, at the web page of this paper: <http://abouthydrology.blogspot.it/2015/07/site-specific-long-wave-radiation.html>.

The regressors we have selected are: mean annual air temperature, relative humidity, precipitation, and altitude. The models that we use for the three parameters are presented in equations (6), (7), and (8):

$$X = a_X + \sum_{k=1}^N \alpha_k \cdot r_k + \epsilon_X \quad (6)$$

$$Y = a_Y + \sum_{k=1}^N \beta_k \cdot r_k + \epsilon_Y \quad (7)$$



$$Z = a_Z + \sum_{k=1}^N \gamma_k \cdot r_k + \epsilon_Z \quad (8)$$

235 where  $N=4$  is the number of regressors (annual mean air temperature, relative humidity, precipitation,  
236 and altitude);  $r_k$  with  $k=1, \dots, 4$  are the regressors;  $a_X$ ,  $a_Y$ , and  $a_Z$  are the intercepts;  $\alpha_k$ ,  $\beta_k$ , and  $\gamma_k$  are  
237 the coefficients; and  $\epsilon_X$ ,  $\epsilon_Y$ , and  $\epsilon_Z$  are the normally distributed errors. Once the regression parameters are  
238 determined, the end-user can estimate site specific X, Y and Z parameter values for any location by simply  
239 substituting the values of the regressors in the model formulations.

240 The performances of the  $L_{\perp}$  models using parameters assessed by linear regression are evaluated through  
241 the leave-one-out cross validation (Efron and Efron, 1982). We use 23 stations as training-sets for equations  
242 (6), (7), and (8) and we perform the model verification on the remaining station. The procedure is repeated for  
243 each of the 24 stations.

244 The cross validation results for all  $L_{\perp}$  models and for all stations are presented in figures (8) and (10), grouped  
245 by classes of latitude and longitude, respectively. They report the KGE comparison between the  $L_{\perp}$  models  
246 with their original parameters (in red) and with the regression model parameters (in blue).

247 In general, the use of parameters estimated with regression model gives a good estimation of  $L_{\perp}$ , with KGE  
248 values of up to 0.97. With respect to the classic formulation, model performance with regression parameters  
249 improved for all the models, in particular for model 8 in which the KGE improved from a minimum of 0.16 for  
250 the classic formulation to a maximum of 0.97.

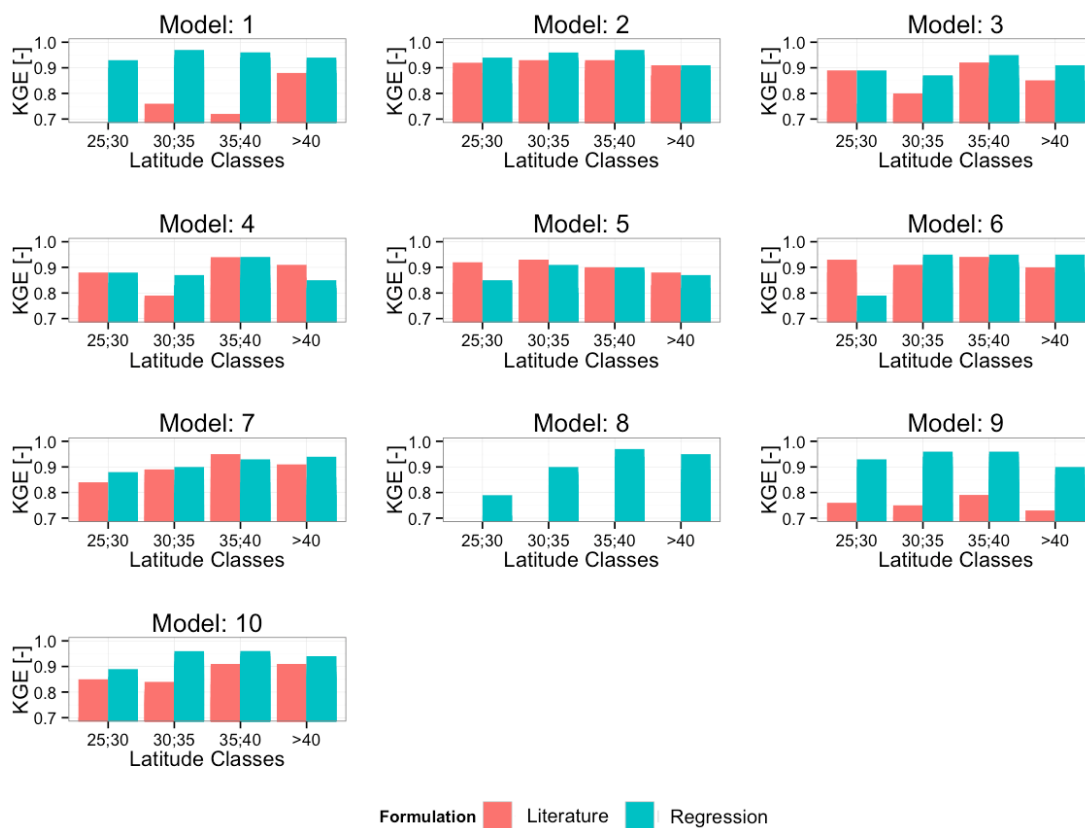


**Figure 8:** Comparison between model performances obtained with regression and classic parameters: the KGE values shown are those above 0.7 and results are grouped by latitude classes.

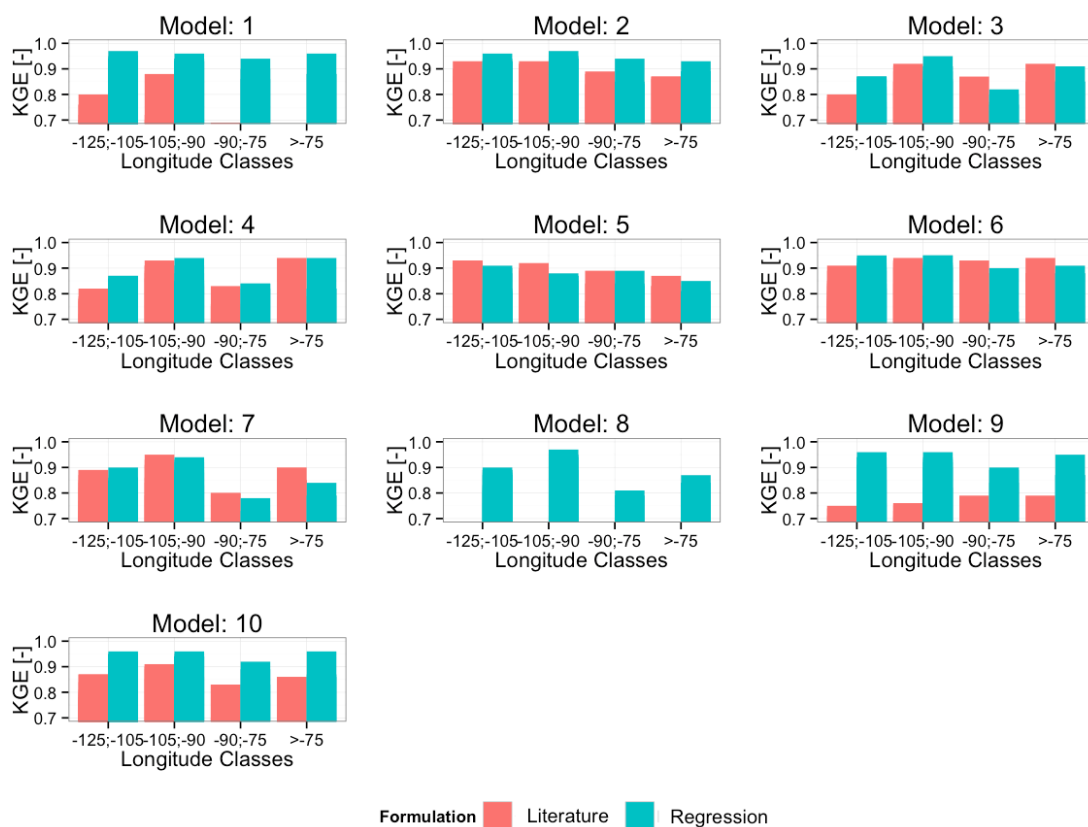


**Figure 9:** Comparison between model performances obtained with regression and classic parameters: the KGE values shown are those above 0.7 and results are grouped by longitude classes.



#### 251 4.5 Verification of the $L_{\uparrow}$ model

252 Figure 10 presents the results of the  $L_{\uparrow}$  simulations obtained using the three different temperatures available at  
253 experimental sites: soil surface temperature (skin temperature), air temperature, and soil temperature (mea-  
254 sured at 4 cm below the surface). The figure shows the performances of the  $L_{\uparrow}$  model for the three different  
255 temperatures used in terms of KGE, grouping all the stations for the whole simulation period according to  
256 season. This highlights the different behaviors of the model for periods where the differences in the three tem-  
257 peratures are larger (winter) or negligible (summer). The values of soil emissivity are assigned according the  
258 soil surface type, according to Table 4 (Brutsaert, 2005).

259 The best fit between measured and simulated  $L_{\uparrow}$  is obtained with the surface soil temperature, with an all-  
260 season average KGE of 0.80. Unfortunately, the soil surface temperature is not an easily available measurement.  
261 In fact, it is available only for 8 sites of the 24 in the study area. Very good results are also obtained using the  
262 air temperature, where the all-season average KGE is around 0.76. The results using air temperature present  
263 much more variance compared to those obtained with the soil surface temperature. However, air temperature  
264 (at 2 m height) is readily available measure, in fact it is available for all 24 sites.

265 The use soil temperature at 4 cm depth provides the least accurate results for our simulations, with an  
266 all-season average KGE of 0.46. In particular, the use of soil temperature at 4 cm depth during the winter is  
267 not able to capture the dynamics of  $L_{\uparrow}$ . It does, however, show a better fit during the other seasons. This could  
268 be because during the winter there is a substantial difference between the soil and skin temperatures, as also  
269 suggested in Park et al. (2008).

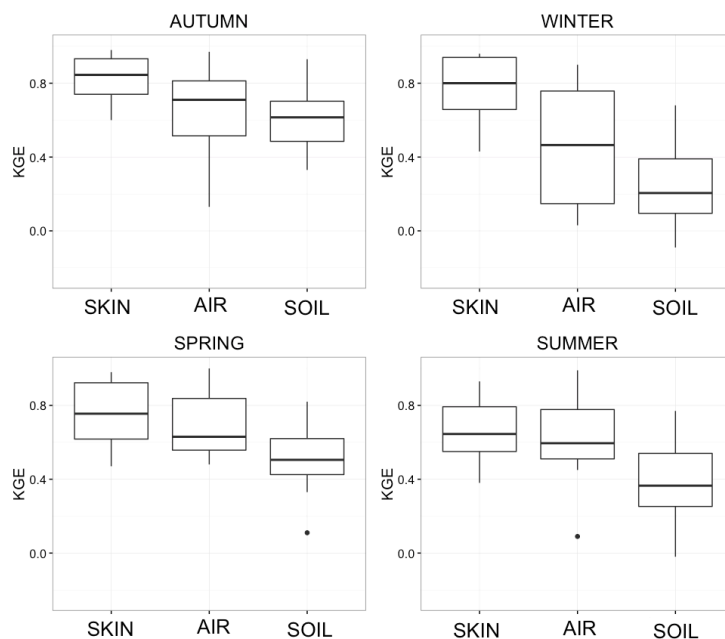


**Figure 10:** Boxplots of the KGE values obtained by comparing modeled upwelling longwave radiation, computed with different temperatures (soil surface temperature (SKIN), air temperature (AIR), and soil temperature (SOIL)), against measured data. Results are grouped by seasons.

## 270 5 Conclusions

271 This paper presents the LWRB package, a new modeling component integrated into the JGrass-NewAge system  
272 to model upwelling and downwelling longwave radiation. It includes ten parameterizations for the computation  
273 of  $L_{\downarrow}$  longwave radiation and one for  $L_{\uparrow}$ . The package uses all the features offered by the JGrass-NewAge  
274 system, such as algorithms to estimate model parameters and tools for managing and visualizing data in GIS.

275 The LWRB is tested against measured  $L_{\downarrow}$  and  $L_{\uparrow}$  data from twenty-four AmeriFlux test-sites located all  
276 over continental USA. The application for  $L_{\downarrow}$  longwave radiation involves model parameter calibration, model  
277 performance assessment, and parameters sensitivity analysis. Furthermore, we provide a regression model that  
278 estimates optimal parameter sets on the basis of local climatic variables, such as mean annual air temperature,  
279 relative humidity, and precipitation. The application for  $L_{\uparrow}$  longwave radiation includes the evaluation of model  
280 performance using three different temperatures.

281 The main achievements of this work include: i) a broad assessment of the classic  $L_{\downarrow}$  longwave radiation  
282 parameterizations, which clearly shows that the Idso (1981) and Brunt (1932) models are the more robust  
283 and reliable for all the test sites, confirming previous results; ii) a site specific assessment of the  $L_{\downarrow}$  longwave  
284 radiation model parameters for twenty-four AmeriFlux sites that improved the performances of all the models;  
285 iii) the set up of a regression model that provides an estimate of optimal parameter sets on the basis climatic  
286 data; iv) an assessment of  $L_{\uparrow}$  model performances for different temperatures (skin temperature, air temperature,  
287 and soil temperature at 4 cm below surface), which shows that the skin and the air temperature are better



288 proxy for the  $L_{\uparrow}$  longwave radiation.

289 The integration of the package into JGrass-NewAge will allow users to build complex modeling solutions  
290 for various hydrological scopes. In fact, future work will include the link of the LWRB package to the existing  
291 components of JGrass-NewAge to investigate  $L_{\downarrow}$  and  $L_{\uparrow}$  effects on evapotranspiration, snow melting, and glacier  
292 evolution.

## 293 ACKNOWLEDGEMENTS

294 The authors are grateful to the AmeriFlux research community for providing the high-quality public data sets.  
295 In particular, we want to thank the principal investigators of each site: Shirley Kurc Papuga (AZ), Tilden  
296 P. Meyers (AZ), Russ Scott (AZ), Tom Kolb (AZ), Sonia Wharton (CA), Dennis D. Baldocchi (CA), Jordan  
297 G. Barr (FL), Vic C. Engel (FL), Jose D. Fuentes (FL), Joseph C. Zieman (FL), David Y. Hollinger (ME), Joe  
298 McFadden (MN), John M. Baker (MN), Timothy J. Griffis (MN), Lianhong Gu (MO), Kenneth L. Clark (NJ),  
299 Dave Billesbach (OK), James A. Bradford (OK), Margaret S. Torn (OK), James L. Heilman (TX), Ken Bible  
300 (WA), Sonia Wharton (WA). The authors thank the CLIMAWARE Project, of the University of Trento (Italy),  
301 and the GLOBAQUA Project, which have supported their research.

## 302 Replicable Research

303 In order that interested researchers may replicate or extend our results, our codes are made available at  
304 <https://github.com/geoframecomponents>.  
305 Instructions for using the code can be found at:  
306 <http://geoframe.blogspot.co.uk/2016/04/lwrp-component-latest-documentation.html>.  
307 Regression of parameters were performed in R and are available at  
308 [https://github.com/GEOframeOMSProjects/OMS\\_Project\\_LWRB/blob/master/docs/Regression.R](https://github.com/GEOframeOMSProjects/OMS_Project_LWRB/blob/master/docs/Regression.R)

## 309 References

- 310 L Alados-Arboledas, J Vida, and FJ Olmo. The estimation of thermal atmospheric radiation under cloudy  
311 conditions. *International journal of climatology*, 15(1):107–116, 1995.
- 312 Anders Knutsson Ångström. *A study of the radiation of the atmosphere: based upon observations of the nocturnal*  
313 *radiation during expeditions to Algeria and to California*, volume 65. Smithsonian Institution, 1915.
- 314 John A Augustine, John J DeLuisi, and Charles N Long. Surfrad-a national surface radiation budget network  
315 for atmospheric research. *Bulletin of the American Meteorological Society*, 81(10):2341–2357, 2000.
- 316 John A Augustine, Gary B Hodges, Christopher R Cornwall, Joseph J Michalsky, and Carlos I Medina. An  
317 update on surfrad-the gcos surface radiation budget network for the continental united states. *Journal of*  
318 *Atmospheric and Oceanic Technology*, 22(10):1460–1472, 2005.



- 319 Dennis Baldocchi, Eva Falge, Lianhong Gu, Richard Olson, David Hollinger, Steve Running, Peter Anthoni,  
320 Ch Bernhofer, Kenneth Davis, Robert Evans, et al. Fluxnet: A new tool to study the temporal and spatial  
321 variability of ecosystem-scale carbon dioxide, water vapor, and energy flux densities. *Bulletin of the American*  
322 *Meteorological Society*, 82(11):2415–2434, 2001.
- 323 Jordan G Barr, Vic Engel, Thomas J Smith, and José D Fuentes. Hurricane disturbance and recovery of energy  
324 balance, co<sub>2</sub> fluxes and canopy structure in a mangrove forest of the florida everglades. *Agricultural and*  
325 *Forest Meteorology*, 153:54–66, 2012.
- 326 David Brunt. Notes on radiation in the atmosphere. i. *Quarterly Journal of the Royal Meteorological Society*,  
327 58(247):389–420, 1932.
- 328 Wilfried Brutsaert. On a derivable formula for long-wave radiation from clear skies. *Water Resources Research*,  
329 11(5):742–744, 1975.
- 330 Wilfried Brutsaert. *Hydrology: an introduction*, volume 61. Wiley Online Library, 2005.
- 331 Gaylon S Campbell. *Soil physics with BASIC: transport models for soil-plant systems*, volume 14. Elsevier,  
332 1985.
- 333 Facundo Carmona, Raúl Rivas, and Vicente Caselles. Estimation of daytime downward longwave radiation  
334 under clear and cloudy skies conditions over a sub-humid region. *Theoretical and applied climatology*, 115  
335 (1-2):281–295, 2014.
- 336 John M Chambers, TJ Hastie, et al. *Linear models*, 1992.
- 337 Todd M Crawford and Claude E Duchon. An improved parameterization for estimating effective atmospheric  
338 emissivity for use in calculating daytime downwelling longwave radiation. *Journal of Applied Meteorology*, 38  
339 (4):474–480, 1999.
- 340 O David, JC Ascough, W Lloyd, TR Green, KW Rojas, GH Leavesley, and LR Ahuja. A software engineering  
341 perspective on environmental modeling framework design: The object modeling system. *Environmental*  
342 *Modelling & Software*, 39:201–213, 2013.
- 343 QY Duan, Vijai K Gupta, and Soroosh Sorooshian. Shuffled complex evolution approach for effective and  
344 efficient global minimization. *Journal of optimization theory and applications*, 76(3):501–521, 1993.
- 345 Bradley Efron and B Efron. *The jackknife, the bootstrap and other resampling plans*, volume 38. SIAM, 1982.
- 346 GN Flerchinger. The simultaneous heat and water (shaw) model: Technical documentation, northwest watershed  
347 research center, usda agricultural research service, boise. Technical report, Idaho, Technical Report NWRC  
348 2000-09, 37 pp, 2000.
- 349 GN Flerchinger, Wei Xaio, Danny Marks, TJ Sauer, and Qiang Yu. Comparison of algorithms for incoming  
350 atmospheric long-wave radiation. *Water resources research*, 45(3), 2009.



- 351 G Formetta, R Rigon, JL Chávez, and O David. Modeling shortwave solar radiation using the jgrass-newage  
352 system. *Geoscientific Model Development*, 6(4):915–928, 2013.
- 353 G Formetta, A Antonello, S Franceschi, O David, and R Rigon. Hydrological modelling with components: A  
354 gis-based open-source framework. *Environmental Modelling & Software*, 55:190–200, 2014a.
- 355 G Formetta, O David, and R Rigon. Testing site-specific parameterizations of longwave radiation integrated  
356 in a gis-based hydrological model. *International Environmental Modelling and Software Society (iEMSs) 7th  
357 Intl. Congress on Env. Modelling and Software, San Diego, CA, USA, Daniel P. Ames, Nigel W.T. Quinn  
358 and Andrea E. Rizzoli (Eds.)*, 2014b.
- 359 Hoshin V Gupta, Harald Kling, Koray K Yilmaz, and Guillermo F Martinez. Decomposition of the mean  
360 squared error and nse performance criteria: Implications for improving hydrological modelling. *Journal of  
361 Hydrology*, 377(1):80–91, 2009.
- 362 JL Hatfield, R JI Reginato, and SB Idso. Comparison of long-wave radiation calculation methods over the  
363 united states. *Water Resources Research*, 19(1):285–288, 1983.
- 364 Lauren E Hay, George H Leavesley, Martyn P Clark, Steve L Markstrom, Roland J Viger, and Makiko Umemoto.  
365 Step wise, multiple objective calibration of a hydrologic model for a snowmelt dominated basin1, 2006.
- 366 Sherwood B Idso. A set of equations for full spectrum and 8-to 14- $\mu\text{m}$  and 10.5-to 12.5- $\mu\text{m}$  thermal radiation  
367 from cloudless skies. *Water resources research*, 17(2):295–304, 1981.
- 368 Sherwood B Idso and Ray D Jackson. Thermal radiation from the atmosphere. *Journal of Geophysical Research*,  
369 74(23):5397–5403, 1969.
- 370 MOSES G Iziomon, HELMUT Mayer, and ANDREAS Matzarakis. Downward atmospheric longwave irradi-  
371 ance under clear and cloudy skies: Measurement and parameterization. *Journal of Atmospheric and Solar-  
372 Terrestrial Physics*, 65(10):1107–1116, 2003a.
- 373 MOSES G Iziomon, HELMUT Mayer, and ANDREAS Matzarakis. Downward atmospheric longwave irradi-  
374 ance under clear and cloudy skies: Measurement and parameterization. *Journal of Atmospheric and Solar-  
375 Terrestrial Physics*, 65(10):1107–1116, 2003b.
- 376 I Juszak and F Pellicciotti. A comparison of parameterizations of incoming longwave radiation over melting  
377 glaciers: model robustness and seasonal variability. *Journal of Geophysical Research: Atmospheres*, 118(8):  
378 3066–3084, 2013.
- 379 I Keding. *Klimatologische Untersuchung ueber die atmosphaerische Gegenstrahlung und Vergleich vom Berech-  
380 nungsverfahren anhand langjaehriger Messungen im Oberrheintal*. Offenbach am Main: Selbstverlag des  
381 Deutschen Wetterdienstes, 1989.



- 382 FM Kelliher, DJ Ross, BE Law, DD Baldocchi, and NJ Rodda. Limitations to carbon mineralization in litter  
383 and mineral soil of young and old ponderosa pine forests. *Forest Ecology and Management*, 191(1):201–213,  
384 2004.
- 385 Jeffrey R Key and Axel J Schweiger. Tools for atmospheric radiative transfer: Streamer and fluxnet. *Computers  
386 & Geosciences*, 24(5):443–451, 1998.
- 387 Francis X Kneizys, EP Shettle, LW Abreu, JH Chetwynd, and GP Anderson. Users guide to lowtran 7. Technical  
388 report, DTIC Document, 1988.
- 389 Thomas Konzelmann, Roderik SW van de Wal, Wouter Greuell, Richard Bintanja, Edwin AC Henneken, and  
390 Ayako Abe-Ouchi. Parameterization of global and longwave incoming radiation for the greenland ice sheet.  
391 *Global and Planetary change*, 9(1):143–164, 1994.
- 392 Egbert Giles Leigh Jr. *Tropical Forest Ecology: A View from Barro Colorado Island: A View from Barro  
393 Colorado Island*. Oxford University Press, 1999.
- 394 Shelley MacDonell, Lindsey Nicholson, and Christophe Kinnard. Parameterisation of incoming longwave radia-  
395 tion over glacier surfaces in the semiarid andes of chile. *Theoretical and applied climatology*, 111(3-4):513–528,  
396 2013.
- 397 Sami Niemelä, Petri Räisänen, and Hannu Savijärvi. Comparison of surface radiative flux parameterizations:  
398 Part i: Longwave radiation. *Atmospheric Research*, 58(1):1–18, 2001.
- 399 Gi-Hyeon Park, Xiaogang Gao, and Soroosh Sorooshian. Estimation of surface longwave radiation components  
400 from ground-based historical net radiation and weather data. *Journal of Geophysical Research: Atmospheres  
401 (1984–2012)*, 113(D4), 2008.
- 402 Christian Plüss and Atsumu Ohmura. Longwave radiation on snow-covered mountainous surfaces. *Journal of  
403 Applied Meteorology*, 36(6):818–824, 1997.
- 404 AJ Prata. A new long-wave formula for estimating downward clear-sky radiation at the surface. *Quarterly  
405 Journal of the Royal Meteorological Society*, 122(533):1127–1151, 1996.
- 406 E Rotenberg, Y Mamane, and JH Joseph. Long wave radiation regime in vegetation-parameterisations for  
407 climate research. *Environmental modelling & software*, 13(3):361–371, 1998.
- 408 M Sugita and W Brutsaert. Comparison of land surface temperatures derived from satellite observations with  
409 ground truth during fire. *International Journal of Remote Sensing*, 14(9):1659–1676, 1993a.
- 410 Michiaki Sugita and Wilfried Brutsaert. Cloud effect in the estimation of instantaneous downward longwave  
411 radiation. *Water Resources Research*, 29(3):599–605, 1993b.
- 412 GN Wilkinson and CE Rogers. Symbolic description of factorial models for analysis of variance. *Applied  
413 Statistics*, pages 392–399, 1973.



414 Jingfeng Xiao, Qianlai Zhuang, Beverly E Law, Jiquan Chen, Dennis D Baldocchi, David R Cook, Ram Oren,  
415 Andrew D Richardson, Sonia Wharton, Siyan Ma, et al. A continuous measure of gross primary production  
416 for the conterminous united states derived from modis and ameriflux data. *Remote sensing of environment*,  
417 114(3):576–591, 2010.